aPKC-mediated displacement and actomyosin-mediated retention polarize Miranda in *Drosophila* neuroblasts

Matthew Hannaford[1], Anne Ramat[1], Nicolas Loyer[1] and Jens Januschke[1#]

[1]Cell & Developmental Biology, School of Life Sciences, University of Dundee, Dundee, UK

correspondence: j.januschke@dundee.ac.uk

(4100 words, 5 figures, 6 figure supplements and 13 movies)

SUMMARY

Cell fate generation can rely on the unequal distribution of molecules during progenitor cell division in the nervous system of vertebrates and invertebrates. Here we address asymmetric fate determinant localization in the developing *Drosophila* nervous system, focussing on the control of asymmetric Miranda distribution in larval neuroblasts. We used live imaging of neuroblast polarity reporters at endogenous levels of expression to address Miranda localization during the cell cycle. We reveal that the regulation and dynamics of cortical association of Miranda in interphase and mitosis are different. In interphase Miranda binds directly to the plasma membrane. At the onset of mitosis, Miranda is phosphorylated by aPKC and displaced from the PM. After nuclear envelope breakdown asymmetric localization of Miranda requires actomyosin activity. Therefore, Miranda phosphorylation by aPKC and differential binding to the actomyosin network are required at distinct phases of the cell cycle to polarize fate determinant localization.

INTRODUCTION

The development of the central nervous system depends on asymmetric cell divisions for the balanced production of progenitor as well as differentiating cells. During vertebrate and invertebrate neurogenesis, cell fates can be established through the unequal inheritance of cortical domains or fate determinants during asymmetric progenitor divisions (Knoblich 2008; Doe 2008; Marthiens & ffrench-Constant 2009; Alexandre et al. 2010).

An important step in asymmetric cell division is the establishment of a polarity axis. Asymmetrically dividing *Drosophila* neuroblasts (NBs) establish an axis of polarity at the onset of mitosis. Like in many other polarized cells, this depends on the activity of the Par complex (Goldstein & Macara 2007). As NBs enter prophase, the Par complex including Par3/Bazooka (Baz), aPKC and Par-6 assembles at the apical NB pole, which drives the localization of fate determinants to the opposite NB pole establishing the apico basal polarity axis (Wodarz et al. 1999; Wodarz et al. 2000; Rolls et al. 2003; Petronczki & Knoblich 2001; Betschinger et al. 2003; Homem & Knoblich 2012; Prehoda 2009).

Upon NB division, the basally localized fate determinants segregate to the daughter cell that commits to differentiation. For this to happen correctly, two adapter proteins, Partner of Numb (Pon, Lu et al. 1998) and Miranda (Mira, Ikeshima-Kataoka et al. 1997; Shen et al. 1997), are required. While Pon localizes the Notch signaling regulator Numb (Uemura et al. 1989; Lu et al. 1998), Mira localizes the homeobox transcription factor Prospero (Pros) and

the translational repressor Brat to the basal NB cortex in mitosis (Ikeshima-Kataoka et al. 1997; Betschinger et al. 2006; C.-Y. Lee et al. 2006). In the absence of Mira, fate determination is impaired and tumor-like growth can occur in larval NB lineages (Ikeshima-Kataoka et al. 1997; Caussinus & Gonzalez 2005).

How polarized fate determinant localization in mitotic NBs is achieved is a long-standing question and despite being a well-studied process, this mechanism is not fully understood. In embryonic NBs, Mira localization requires actin (Shen et al. 1998) and myosin activity since mutation in the myosin regulatory light chain *spaghetti squash* (*sqh)* (Barros et al. 2003) or the Myosin VI gene *jaguar* (Petritsch et al. 2003) to lead to Mira localization defects. Furthermore, in embryos injected with the Rho kinase (ROCK) inhibitor Y-27632, Mira does not achieve a polarized distribution, which was rescued by the expression of a phospho-mimetic *sqh* allele. This led to the proposal that Myosin II plays a critical role in Mira localization and aPKC affects Mira localization indirectly through regulating Myosin II (Barros et al. 2003).

However, it was later shown that Y-27632 can inhibit aPKC directly and that Mira is a substrate of aPKC (Atwood & Prehoda 2009; Wirtz-Peitz et al. 2008). In fact many aPKC substrates including Numb and Mira contain a basic and hydrophobic (BH) motif that can be phosphorylated by aPKC. Upon phosphorylation the substrates are no longer able to directly bind phospholipids of the plasma membrane (PM, Bailey & Prehoda 2015; Smith et

al. 2007; Dong et al. 2015). Asymmetric Mira localization in mitotic NBs can in principle be explained by keeping the activity of aPKC restricted to the apical pole (Atwood & Prehoda 2009). However, is less clear what the contribution of the actomyosin network to polarized Mira localization is.

Intriguingly, Mira localizes uniformly to the cortex of larval brain NBs in interphase (Sousa-Nunes et al. 2009) before becoming basally restricted in mitosis. The function and regulation of interphase Mira are unknown. In embryonic NBs in interphase, Mira and its cargo Pros localize to the apical cortex (Spana & Doe 1995) and Pros is found in the nucleus of interphase *mira* mutant NBs (Matsuzaki et al. 1998). Given that the levels of nuclear Pros in NBs are important for the regulation of entry and exit from quiescence and NB differentiation (Lai & Doe 2014), interphase Mira localization might be important in this context.

To reveal the regulation of interphase Mira, we set out to determine differences and similarities in the parameters of Mira binding in interphase and mitosis and the transition between the two different localizations. Using fluorescent reporters of the Par complex and Mira at endogenous levels of expression, we reveal that cortical Mira localization is differently controlled in interphase, where it uniformly binds to the PM and after nuclear envelope breakdown (NEB), when actomyosin activity becomes important.

RESULTS

Uniform Miranda is cleared from the cortex during prophase and Miranda reappears asymmetrically after NEB

We first confirmed in larval NBs that Mira localizes uniformly to the cortex in interphase (**Figure 1A**) and co-localizes with its cargo Pros in interphase and mitosis (**Figure 1 supplement 1**). We further stained *mira* mutant NBs for Mira and Pros. In these cells, Pros is found in the nucleus in interphase (**Figure 1 supplement 1**). These results are consistent with a role of Mira in regulation Pros localization not only in mitosis (Ikeshima-Kataoka et al. 1997), but also potentially during interphase. We therefore sought to address the regulation of cortical Mira in interphase and mitosis and the transition between these localizations.

To accurately monitor *in vivo* the dynamics of this transition, we used a BAC construct in which Mira was tagged at its C-terminus with mCherry (Ramat et al. 2017; **Figure 1 supplement 2**). This tagged Mira recapitulated uniform cortical localization in interphase (**Figure 1B**, **-**33 to NEB) and polarized localization to the basal pole in mitosis (**Figure 1B**, +4), with a 2.5-fold increase in intensity (n=5, **Figure 1B'**). This transition occurred in two distinct steps. Firstly, during prophase, after Mira was rapidly excluded from the apical pole where Baz (**Movie S1**) or aPKC (**Movie S2**) started localizing (**Figure 1B -**8 to NEB, **B'** -15). Thereafter, Mira was progressively cleared from most of the rest of the cortex in an apical-to-basal direction (**Figure 1B, B'** -4, -1, respectively to NEB). Secondly, following NEB, Mira reappeared at

the cortex in a basal crescent after NEB (**Figure 1B ,B'** +4, +5 respectively). We further recapitulated these steps using overexpression of GFP::Mira and by antibody staining of endogenous, non-tagged Mira. The Mira antibody revealed colcemid insensitive cortical localization in interphase, which was lost in *mira* mutant NBs (**Figure 1 supplement 3**). Thus, endogenous Mira also localizes to the cortex independently of microtubules. In conclusion, Mira transitions from a uniform to a polarized localization by first being cleared form most of the cortex during prophase, and only upon NEB reappearing in a basal crescent (**Figure 1C**).

Actomyosin is required for the establishment and maintenance of Miranda crescents after NEB

In embryonic NBs, Mira localization is sensitive to F-actin disruption in mitosis (Shen et al. 1998). We reasoned that this could be due to defective Mira clearance in prophase and/or defective Mira reappearance at the basal cortex after NEB. We tested this by disrupting the actin network of larval NBs with Latrunculin A (LatA). Despite efficiently disrupting F-actin (**Figure 2 supplement**) and causing cytokinesis failure (**Figure 2A,** 3:02, related to **Movie S3**), LatA treatment affected neither uniform cortical localization of Mira in interphase (**Figure 2A,** 2:06) nor its clearance during prophase (**Figure 2A,** 2:21). In contrast, Mira failed to relocalize to a basal crescent following NEB in LatA-treated NBs (**Figure 2A,** 2:33). We next tested whether, in addition to crescent establishment, F-Actin controlled crescents maintenance. To this end, we arrested NBs with colcemid in metaphase (at

141 which point Mira crescents are established), after which we treated them with
142 LatA. Again, LatA caused Mira to relocalize to the cytoplasm (**Figure 2A**).
143 Importantly, this relocalization is unlikely to be due to Mira being "swept off"
144 the cortex by cortical aPKC, which redistributes from an apical crescent to the
145 entire cortex following LatA treatment (**Figure 2 supplement**). This is
146 evident since unlike the gradual apical-to-basal clearance of Mira during
147 prophase (**Figure 1B**), basal Mira crescents fall off the cortex homogenously
148 upon LatA treatment (**Figure 2 supplement**). Furthermore, Mira falls off the
149 cortex 2.8±1min (n=13) before aPKC (**Movie S4**) or Baz become detectable
150 at the basal cortex (**Figure 2 supplement**). Therefore, an intact actin
151 network is required to establish and maintain asymmetric Mira localization in
152 mitotic larval NBs.
153
154 Myosin activity has been proposed to be required for Mira localization
155 (Petritsch et al. 2003; Barros et al. 2003). We tested next which step of Mira
156 localization involved Myosin. Myosin motor activity relies on the
157 phosphoregulation of myosin regulatory light chain, encoded by the *sqh* gene
158 in *Drosophila* (Jordan & Karess 1997), which we disrupted by applying ML-7,
159 a specific inhibitor of the myosin light chain kinase (MLCK, Bain et al. 2003).
160 As with LatA, the ML-7 treatment in cycling neuroblasts affected neither
161 uniform cortical localization of Mira in interphase (**Figure 2B,** 0') nor its
162 clearance during prophase (**Figure 2B,** 138-278') but resulted in failure to
163 establish a basal crescent after NEB, which was restored upon drug washout
164 (**Figure 2B**, 328'). In colcemid-arrested NBs, the ML-7 treatment also

resulted in Mira redistributing from the basal crescent to the cytoplasm, which was restored upon ML-7 washout. Furthermore, unlike LatA treatment, ML-7 did not cause the Par complex to redistribute to the entire cortex (**Figure 2C, Movie S5**). Finally, as in (Das & Storey 2014), we demonstrated the specificity of the effect of ML-7 by counteracting its effect with a phosphomimetic version of Myosin regulatory light chain, Sqh. Overexpressing a phosphomimetic version of Sqh (Sqh^{EE}, (Winter et al. 2001) significantly delayed loss of cortical Mira after ML-7 addition in colcemid arrested NBs (**Figure 2D, Movie S6**).

In conclusion, the contribution of F-Actin (Shen et al. 1998) and Myosin (Petritsch et al. 2003; Barros et al. 2003) to asymmetric Mira localization is linked to the relocalization of Mira and its maintenance at the basal cortex following NEB, but not to the control of uniform cortical localization in interphase or to clearance of Mira during prophase.

Defective clearance of interphase cortical Miranda by aPKC results in the persistence of uniform Miranda in mitosis.

NBs mutant for aPKC also fail to asymmetrically localize Mira in mitosis (Rolls et al. 2003), prompting us to investigate which aspect of Mira localization involved aPKC in larval NBs. Like in controls, Mira localized uniformly to the cortex of *apkc*^{k06403} (Wodarz et al. 2000) mutant NBs in interphase. However, it did not clear from the cortex during prophase and instead remained uniformly localized throughout mitosis (**Movie S7**, **Figure 3A**). Additionally, expressing a constitutively active form of aPKC, $aPKC^{\Delta N}$, resulted in the loss of

uniform cortical Mira binding in interphase (**Figure 3 supplement**). These results show that during prophase, aPKC negatively regulates the uniform cortical localization of Mira observed in interphase. They also suggest that the failure to asymmetrically localize Mira in mitosis in aPKC mutants is due to defective clearance in prophase resulting in the abnormal persistence of uniform cortical Mira throughout mitosis.

We reasoned that, if this were the case, Mira localization in interphase should have the same characteristics as Mira localization in metaphase upon loss of function of aPKC. Consistent with this view, unlike Mira localization in mitosis, but similar to Mira localization in interphase (**Figure 2A**), Mira localization to the cortex in mitosis was insensitive to LatA treatment in NBs depleted for aPKC (**Figure 3 supplement**). To corroborate these results we used fluorescence redistribution after photo-bleaching (FRAP) to analyze the lateral diffusion/cytoplasmic exchange dynamics of Mira (**Figure 3B**).

In controls, Mira redistributed about three times faster in interphase compared to mitosis (**Figure 3C, C'**), suggesting that Mira dynamics are indeed a relevant characteristic to analyze cell cycle-dependent control of Mira localization. Yet, in apparent contradiction with our proposition, while Mira redistribution became faster when aPKC was knocked down by RNAi (or Lgl^{3A} overexpression, known to inhibit aPKC, Betschinger et al. 2003), these conditions did not result in Mira redistribution in mitosis becoming as fast as in interphase (**Figure 3C, C'**). However, changes in the actin network caused

by progression through the cell cycle (Ramanathan et al. 2015) can influence dynamics of membrane-associated proteins in general (Heinemann et al. 2013). This is also the case in NBs, as a photo-convertible membrane-associated reporter that attaches to the entire NB PM via a myristoylation signal (myr-Eos) showed similar slowing of dynamics in mitosis compared to interphase (~four-fold, **Figure 3D, D'**).

Thus, this general cell cycle-driven change of dynamics may account for the difference between Mira redistribution in interphase and in mitosis in aPKC-impaired NBs. We tested this by cancelling this general change by treating mitotic NBs with LatA, which resulted as expected in myr-Eos dynamics falling into ranges similar to interphase (**Figure 3D, D'**). In aPKC-impaired NBs, the same LatA treatment resulted in Mira redistribution rates becoming as fast as in interphase (Figure 3C, C'), suggesting that aPKC loss of function indeed leads to the persistence of the same dynamics as in interphase (**Figure 3C, C'**). Importantly, myr-Eos dynamics were not sensitive to Lgl^{3A} overexpression alone, arguing against the possibility that aPKC impairment causes general changes in the cortex that could explain accelerated redistribution of Mira in this condition.

In conclusion, instead of being cleared, Mira persists throughout mitosis with the same actin-insensitive uniform localization and the same dynamics as in interphase in *apkc* mutant NBs.

237 **Miranda binds uniformly to the plasma membrane in interphase**

238 In *Drosophila* S2 cells Mira binds directly to phospholipids of the PM via its BH
239 motif and the ability to bind the PM is abolished upon phosphorylation of this
240 motif by aPKC (Bailey & Prehoda, 2015). Our results, that Mira cortical
241 localization in interphase is actin-independent and that its clearance in
242 prophase is aPKC dependent, suggest that in interphase Mira is retained
243 uniformly at the PM by its BH motif.

244

245 Five aPKC phosphorylation sites have been identified in Mira, only one of
246 which Serine 96 (S96) directly resides in the BH motif. To investigate its
247 influence on dynamic Mira localization in neuroblasts, we used CrispR to
248 generate mCherry-tagged versions of Mira control (S96, ctrl, able to rescue
249 embryonic lethality; see **Figure 1 supplement 2**), a phosphomutant version
250 (S96A, homozygous embryonic lethal), a phosphomimetic version (S96D,
251 homozygous embryonic lethal) - shown *in vitro* to reduce phospholipid
252 binding and Mira recruitment to the PM when overexpressed in S2 cells
253 (Bailey & Prehoda 2015) - and a complete deletion of the BH motif (ΔBH,
254 homozygous embryonic lethal).

255

256 The control, S96, localized uniformly to the cortex in interphase, was cleared
257 from the cortex in prophase and reappeared as a basal crescent after NEB
258 (**Figure 4A, Movie S8**). In contrast, while S96A localized uniformly to the
259 cortex in interphase, it was not cleared at the onset of prophase when it
260 presented a transient apical enrichment, perhaps explainable by abnormally

stable interactions with apically localized aPKC. After NEB, S96A, localized however uniformly to the cortex (**Figure 4A**, **Movie S9**), which occurred independently of F-actin (**Figure 4B**). Furthermore, S96D did not localize to the cortex in interphase and instead accumulated predominantly on cortical microtubules, as evidenced by its relocalization to the cytoplasm upon colcemid treatment (**Figure 4B**). Nonetheless, S96D always localized asymmetrically at the cortex following NEB, despite at reduced levels (**Figure 4A**, **Movie S10**).

Finally, deletion of the BH motif abolished both uniform cortical localization in interphase and asymmetric cortical localization after NEB (**Figure 4A**, **Movie S11,** see **Figure 4C** for quantification and **Figure 4D** for summary of the localization of the different Mira mutants in interphase and mitosis). Therefore, our findings are consistent with Mira being bound via its BH motif to the phospholipids of the PM in interphase, and that phosphorylation of S96 by aPKC in prophase disrupts this interaction.

Mira crescent size is affected by a Y-27632-sensitive mechanism that operates before NEB

So far, our results demonstrate that in interphase Mira binds uniformly the PM, from which it is cleared by aPKC at the onset of prophase. However, upon NEB Mira localization requires actomyosin. This raises the question whether aPKC contributes to Mira asymmetric localization after NEB. Temporally controlled inactivation can be achieved with temperature sensitive

(ts) alleles or small molecule inhibition. We find that the available ts allele of aPKC (Guilgur et al. 2012) is hypomorphic already at permissive temperature resulting in Mira localization defects (not shown). Therefore, we made use of the non-specific effects of the ROCK inhibitor Y-27632, which inhibits aPKC with an IC_{50} of 10µM (Atwood & Prehoda 2009). When we added 50µM of Y-27632 to already polarized NBs, after 1h in the presence of the drug, we did not detect any significant changes in Mira or aPKC crescent size (n=22, **Figure 5A,** and **Figure 5 supplement**).

In striking contrast, when we added half that dose to cycling NBs, while aPKC crescent size was comparable to controls (**Fig 5 supplement**) Mira crescents formed, but were significantly enlarged. As a consequence daughter cell size was also increased (n=12, **Figure 5B, B'**). Intriguingly, such enlarged crescents were LatA and ML-7 sensitive (**Figure 5C**, see **Figure 5D** for Mira crescent size quantification), both indicators that enlarged Mira crescents were not due to lack of phosphorylation of Mira by aPKC. However, when we titrated the Y-27632 concentration to induce uniform cortical Mira when added to cycling NBs, Mira became uniformly cortical and was insensitive to LatA treatment in the presence of 200µM Y-27632, suggesting that this concentration can lead to inhibition of Mira phosphorylation by aPKC (**Movie S12**, n=25 and not shown).

We then treated colcemid arrested NBs with 200µM Y-27632. It took on average 52±11min (n=15) until faint Mira signal became detectable apically. Nevertheless, Mira distribution remained always biased towards the basal pole in the presence of Y-27632, an asymmetry that was lost only when we additionally added LatA, which caused Mira to become uniformly distributed on the PM (**Figure 5E**, **Movie 13**, n=15). Therefore, 200µM Y-27632 when added to colcemid arrested NBs, may have an effect on Mira phosphorylation by aPKC, causing ectopic accumulation of Mira apically. However, given the non-specific nature of Y-27632 especially at high concentrations, a role for aPKC cannot be precisely determined in this way.

Nonetheless, when added at lower concentrations (25µM) before NEB, Y-27632 has an effect on Mira crescent size that is unlikely to be caused by failure of aPKC to phosphorylate Mira.

Discussion

The establishment of different cell fates in the developing nervous system can rely on asymmetric distribution of molecules. In this study, we reinvestigated *in vivo* the precise contributions of aPKC and actomyosin to the localization of the cell fate determinant adapter Mira during the cell cycle of *Drosophila* larval NBs. Using live cell imaging we reveal a stepwise contribution of aPKC and actomyosin to Mira localization. First, Mira was cleared from most of the cortex during prophase; second, Mira came back to the cortex as a basal crescent following NEB (**Figure 1B-C**). We then proceeded to assess the relative contributions of aPKC and actomyosin to these steps. Our study

reveals that the central elements of two models proposed to explain Mira asymmetry, requiring actomyosin (Barros et al. 2003) or involving direct aPKC phosphoregulation (Atwood & Prehoda 2009) are both correct. Our time-resolved analysis further allowed determining when in the cell cycle the proposed mechanisms operate to establish asymmetric fate determinant localization.

During interphase, Mira localization does not require the actin cortex, but the BH motif and Serine 96 (S96) in particular (**Figure 4A**). Thus, in interphase NBs Mira binds with its BH motif to phospholipids of the PM (Bailey & Prehoda 2015). At the onset of prophase Mira is driven off the PM into the cytoplasm by aPKC since mutating S96 to Alanine prevents clearance and F-actin-independent Mira uniformly binding to the PM persists, which is also true in mitotic *apkc* NBs (**Figure 3A**, **Figure 3 supplement**). In contrast, clearance occurs in LatA or ML-7 treated NBs (**Figure 2A**,**B**). Therefore, aPKC rather than actomyosin dependent processes drive Mira clearance.

In the transition from interphase to mitosis, the NBs cytoskeleton gets remodeled, slowing the diffusion of PM-bound proteins (**Figure 3D**). This stage is also sensitive to low doses of the ROCK inhibitor Y-27632 (**Figure 5B**) and the dynamics of Mira clearance appear altered when LatA treated, cycling NBs enter mitosis (**Movie S3**). Thus, as in the *C.elegans* zygote where actomyosin remodeling contributes to the establishment of polarity

(Munro et al. 2004), actomyosin remodeling during prophase might also contribute in NBs to polarize Mira.

After NEB Mira asymmetry requires actomyosin activity (**Figure 2A-D**). Barros et al. (2003) suggested that myosin II is required to exclude Mira from the apical pole pushing Mira it into daughter cells during division. Our results rather suggest that, myosin activity keeps Mira anchored basally (**Figure 2C**). The observation that NEB is a critical time point for basal crescent formation is further in line with the proposition that factors released from the nucleus upon NEB could regulate Mira localization (Zhang et al. 2016). Interestingly, ROCK and MLCK both affect myosin activity (Amano et al. 1996; Ueda et al. 2002; Saitoh et al. 1987; Watanabe et al. 2007) yet the effects of MLCK (ML-7) and ROCK (Y-27632) inhibition on Mira differ (**Figure 2** versus **Figure 5**). In MCDK II cells, Y-27632 and ML-7 treatment has different effects on myosin regulatory light chain phosphorylation (Watanabe et al. 2007). This could result in different effects on myosin activity that may explain the different effects on Mira also in NBs.

Another question raised by our results is whether aPKC contributes to Mira localization following NEB. We attempted to test this by using the ROCK inhibitor Y-27632, also shown to inhibit aPKC (Atwood & Prehoda 2009). High doses (200µM) of Y-27632 applied to cycling NBs recapitulated defective clearance of Mira by aPKC (**Movie S12**), and the same dose applied to already polarized NBs resulted in a partial loss of Mira asymmetry, however

after a ~50min delay (**Figure 5E**, **Movie 13**). Thus, aPKC may be required after NEB to reinforce Mira asymmetry by excluding it apically, as suggested (Atwood & Prehoda 2009). Low doses (25μM) of Y-27632, despite not inhibiting aPKC, affect Mira crescent size in cycling NBs (**Figure 5B**). Thus, Y-27632 also inhibits other aPKC-independent mechanisms, making unclear whether the partial loss of Mira asymmetry in already polarized NBs treated with high Y-27632 is solely due to the disruption of a post-NEB aPKC function. Addressing this question in the future will require specific and temporally controlled aPKC inhibition.

When the BH motif is deleted, Mira cannot form crescents (**Figure 4A**). We recently identified that maintenance of Mira crescents also requires interaction of Mira with its cognate mRNA (Ramat et al. 2017). Thus, establishment of Mira crescents and their maintenance are differently controlled. The BH motif might be important to initiate Mira asymmetric localization, while actomyosin dependent processes contribute to establishment and stabilize Mira in a subsequent maintenance step.

Finally, a question of interest is why would Mira localization to the cortex be controlled by different mechanisms in interphase and mitosis. Mira co-localizes with Pros in interphase (**Figure 1 supplement 1**). It is possible that Mira sequesters Pros, helping to prevent its nuclear localization. In this way Pros induced cell cycle exit could be prevented (Choksi et al. 2006; Lai & Doe 2014). Nuclear Pros is developmentally controlled by hedgehog signaling and

the temporal transcription factor cascade (Chai et al. 2013; Maurange et al. 2008) and regulated by RanGEF BJ1 (Joy et al. 2014). However, the underpinning cell biology is not clear. Being able to regulate Miras interaction with the PM and at the actomyosin cortex differentially might allow controllable segregation of fate determinants to daughter cells while permitting tuning of nuclear Pros levels through its interaction with Mira in interphase.

Materials & Methods

Fly stocks and genetics

Flies were reared on standard corn meal food at 25 degrees. Lines used: (1) Baz::GFP trap (Buszczak et al. 2007); (2) w^{1118} (Bloomington); (3) MARCM: hsFlp tubGal4 UASnlsGFP; FRT42B tubGal80/Cyo and FRT82B gal80 (T. Lee & Luo 1999); (4) worniu-Gal4 (Albertson et al. 2004); (5) UAS-Lgl^{3A}::GFP (Wirtz-Peitz et al. 2008); (6) UAS-Lgl^{3A} (Betschinger et al. 2003); (7)*w1118, y,w, hsp70-flp; tubP-FRT>cd2>FRT-Gal4, UAS-GFP (Gift from* M. Gho); (8) Mz1061 (Ito et al. 1995); (9) UAS-GFP::Mira (Mollinari et al. 2002). (10) FRT82B *mira*^{L44} (Matsuzaki et al. 1998). (10) Df(3R)ora^{I9} (Shen et al. 1997). (11) UAS-aPKC^{RNAi}: *P{y[+t7.7] v[+t1.8]=TRiP.HMS01320}attP2* (BL#34332)*; (12)* Numb::GFP (Couturier et al. 2013); (13) FRT42B *apkc*^{k06403} (Wodarz et al. 2000)*;* (14) UAS-aPKC$^{\Delta N}$; (15) P{UASp-sqh.E20E21}3 (BL#64411); (16) P{10xUAS-IVS-mye::tdEos]attP2 (BL #32226); y[1] w[*]; P{y[+t*] w[+mC]=UAS-Lifeact-Ruby}VIE-19A (BL# 35545); (17) aPKC::GFP (Besson et al. 2015); *Source 1 of Mira::mCherry: BAC{mira::mcherry-MS2}* (Ramat et al. 2017). aPKC^{RNAi} clones were generated by heat-shocking larvae of the genotype *y,w, hsp70-flp; tubP-FRT>cd2>FRT-Gal4, UAS-GFP; P{y[+t7.7] v[+t1.8]=TRiP.HMS01320}attP2*. Heat shocks were performed 24hph and 48hph for 1 hour at 37ºC. MARCM clones were generated by heat shocking L1 larvae for 2h at 37°C.

Generation of Mira alleles: Source 2 of Mira::mCherry: *mira*^{mCherry}; *mira*$^{\Delta BHmCherry}$ (Ramat et al. 2017), *mira*$^{S96A\text{-}mCherry}$ and *mira*$^{S96D\text{-}mCherry}$ are derived from *mira*^{KO} (Ramat et al. 2017). *mira*^{mCherry} was generated by inserting a modified wt genomic locus in which mCherry was fused to the C-terminus following a GSAGS linker into *mira*^{KO}. For *mira*$^{S96D\text{-}mCherry}$: TCG (Serine96) was changed to GAC (aspartic acid). For *mira*$^{S96A\text{-}mCherry}$: TCG was replaced with GCG (alanine). CH322-11-P04 was the source for the *mira* sequences cloned using Gibson assembly into the RIV white vector (Baena-Lopez et al. 2013) that was injected using the attP site in *mira*^{KO} as landing site. *BAC{mira::mcherry-MS2}* (Ramat et al. 2017) **see Figure 1 supplement 2**). While *mira*^{mCherry} behaves similarily to *BAC{mira::mcherry-MS2}* and rescues embryonic lethality, *mira*$^{\Delta BHmCherry}$, *mira*$^{S96A\text{-}mCherry}$ and *mira*$^{S96D\text{-}mCherry}$ are homozygous lethal.

Live imaging: Live imaging was performed as described (Pampalona et al. 2015). Briefly, brains were dissected in collagenase buffer and incubated in collagenase for 20 minutes. Brains were transferred to a drop of fibrinogen (0.2mgml^{-}1, Sigma f-3879) dissolved in Schneider's medium (SLS-04-351Q) on a 25mm Glass bottom dish (WPI). Brains were manually dissociated with needles before the fibrinogen was clotted by addition of thrombin (100Uml^{-1}, Sigma T7513). Schneider's medium supplemented with FCS, Fly serum and Insulin was then added. A 3-4µm slice at the center of the neuroblasts was then imaged every 30-90s using a 100x OIL objective NA1.45 on a spinning disk confocal microscope. Data was processed and analyzed using FIJI (Schindelin et al. 2012). For nuclear volume measurements Imaris was used. All other drugs were added to the media either prior or during imaging: ML-7 (Sigma, I2764, dissolved in water), Y-27632 (Abcam, Ab120129, dissolved in water). Drugs were washed out by media replacement, in the polarity reconstitution assay colcemid concentrations were kept constant throughout the experiments. FRAP experiments were carried out on a Leica SP8 confocal using a 63x NA1.2 APO water immersion objective. To estimate $t_{1/2}$ for the

463 recovery curves we used published curve fitting methods (Rapsomaniki et al.
464 2012).
465
466 *Immunohistochemistry*
467 *Primary cell culture*: Brains were dissected in collagenase buffer and
468 incubated for 20 minutes in collagenase, as for live imaging. Brains were then
469 transferred into supplemented Schneider's medium and manually dissociated
470 by pipetting up and down. Cells were pipetted onto a poly-lysine coated
471 25mm glass bottomed dish and left to adhere for 40 minutes. Schneider's was
472 then replaced with 4% Formaldehyde (Sigma) in PBS and cells were fixed for
473 10 minutes. Cells were permeabilized with 0.1% PBS-Triton for 10 minutes.
474 Cells were then washed with PBS 3x 10minutes before antibody staining
475 overnight at 4ºC. All antibodies were dissolved in PBS-1%Tween. *Whole*
476 *mount brains*: Brains were fixed in 4% Formaldehyde (Sigma) for 20 minutes
477 at room temperature. Primary antibodies: Rabbit anti-Miranda (1:200, gift
478 from C. Gonzalez), Mouse anti-GFP (1:400, Abcam). Rabbit anti-Brat (1:200, a
479 gift from J. Knoblich). Guinea Pig anti-Dpn (1:500 a gift from J. Skeath).
480 Mouse anti-Pros (1:40, DSHB). To stain F-Actin we used Alexa Fluor 488 or
481 561 coupled Phalloidin (Molecular Probes, 5:200) for 20 minutes at room
482 temperature. Secondary antibodies (all from life technologies and raised in
483 donkey: Anti-Rabbit Alexa-594, Anti-Mouse Alexa-488, Anti-Rabbit Alexa-647,
484 Anti-Guinea Pig Alexa-647. Microscopy was performed using a Leica-SP8
485 CLSM (60x Water objective, 1.2) and images were processed using FIJI.
486
487 In all cases the sample size *n* provided reflects all samples collected for one
488 experimental condition. Experimental conditions were repeated at least twice
489 to account for technical and biological variation.
490
491 **Acknowledgements**
492 We thank C. Doe, J. Knoblich, F. Schweisguth, D. StJohnston, F. Matsuzaki, C.
493 Gonzalez, J. Skeath, A. Wodarz, M. Gho and the Kyoto and Bloomington stock
494 centers for reagents and/or protocols. We thank A. Müller, C. Weijer and M.

Gonzalez-Gaitan for critical reading. M.R.H is supported by an MRC PhD studentship. We thank inDroso (http://www.indroso.com) for the generation of *mira*^{attPko} by CrispR and the Dundee imaging facility for excellent support. Work in J.J.'s laboratory is supported by Wellcome and the Royal Society Sir Henry Dale fellowship 100031Z/12/Z. M.R.H is supported by an MRC studentship funded by these grants: G1000386/1, MR/J50046X/1, MR/K500896/1, MR/K501384/1. The tissue imaging facility is supported by the grant WT101468 from Wellcome.

References

Albertson, R. et al., 2004. Scribble protein domain mapping reveals a multistep localization mechanism and domains necessary for establishing cortical polarity. *Journal of Cell Science*, 117(Pt 25), pp.6061–6070.

Alexandre, P. et al., 2010. Neurons derive from the more apical daughter in asymmetric divisions in the zebrafish neural tube. *Nature Neuroscience*, 13(6), pp.673–679.

Amano, M. et al., 1996. Phosphorylation and activation of myosin by Rho-associated kinase (Rho-kinase). *The Journal of biological chemistry*, 271(34), pp.20246–20249.

Atwood, S.X. & Prehoda, K.E., 2009. aPKC phosphorylates Miranda to polarize fate determinants during neuroblast asymmetric cell division. *Current biology : CB*, 19(9), pp.723–729.

Baena-Lopez, L.A. et al., 2013. Accelerated homologous recombination and subsequent genome modification in Drosophila. *Development*.

Bailey, M.J. & Prehoda, K.E., 2015. Establishment of Par-Polarized Cortical Domains via Phosphoregulated Membrane Motifs. *Developmental Cell*, 35(2), pp.199–210.

Bain, J. et al., 2003. The specificities of protein kinase inhibitors: an update. *The Biochemical journal*, 371(Pt 1), pp.199–204.

Barros, C.S., Phelps, C.B. & Brand, A.H., 2003. Drosophila nonmuscle myosin II promotes the asymmetric segregation of cell fate determinants by cortical exclusion rather than active transport. *Developmental Cell*, 5(6), pp.829–840.

Besson, C. et al., 2015. Planar Cell Polarity Breaks the Symmetry of PAR Protein Distribution prior to Mitosis in Drosophila Sensory Organ Precursor Cells. *Current biology : CB*, 25(8), pp.1104–1110.

Betschinger, J., Mechtler, K. & Knoblich, J.A., 2006. Asymmetric segregation of the tumor suppressor brat regulates self-renewal in Drosophila neural stem cells. *Cell*, 124(6), pp.1241–1253.

Betschinger, J., Mechtler, K. & Knoblich, J.A., 2003. The Par complex directs asymmetric cell division by phosphorylating the cytoskeletal protein Lgl. *Nature Cell Biology*, 422(6929), pp.326–330.

534 Buszczak, M. et al., 2007. The carnegie protein trap library: a versatile tool for Drosophila
535 developmental studies. *Genetics*, 175(3), pp.1505–1531.

536 Caussinus, E. & Gonzalez, C., 2005. Induction of tumor growth by altered stem-cell
537 asymmetric division in Drosophila melanogaster. *Nature Genetics*, 37(10), pp.1125–1129.

538 Chai, P.C. et al., 2013. Hedgehog signaling acts with the temporal cascade to promote
539 neuroblast cell cycle exit., 11(2), p.e1001494.

540 Choksi, S.P. et al., 2006. Prospero acts as a binary switch between self-renewal and
541 differentiation in Drosophila neural stem cells. *Developmental Cell*, 11(6), pp.775–789.

542 Couturier, L., Mazouni, K. & Schweisguth, F., 2013. Numb localizes at endosomes and
543 controls the endosomal sorting of notch after asymmetric division in Drosophila. *Current*
544 *biology : CB*, 23(7), pp.588–593.

545 Doe, C.Q., 2008. Neural stem cells: balancing self-renewal with differentiation. *Development*,
546 135(9), pp.1575–1587.

547 Dong, W. et al., 2015. A conserved polybasic domain mediates plasma membrane targeting
548 of Lgl and its regulation by hypoxia. *The Journal of Cell Biology*, 211(2), pp.273–286.

549 Fuerstenberg, S. et al., 1998. Identification of Miranda protein domains regulating
550 asymmetric cortical localization, cargo binding, and cortical release. *Molecular and*
551 *cellular neurosciences*, 12(6), pp.325–339.

552 Goldstein, B. & Macara, I.G., 2007. The PAR proteins: fundamental players in animal cell
553 polarization. *Developmental Cell*, 13(5), pp.609–622.

554 Guilgur, L.G. et al., 2012. Drosophila aPKC is required for mitotic spindle orientation during
555 symmetric division of epithelial cells. *Development*, 139(3), pp.503–513.

556 Homem, C.C.F. & Knoblich, J.A., 2012. Drosophila neuroblasts: a model for stem cell biology.
557 *Development*, 139(23), pp.4297–4310.

558 Ikeshima-Kataoka, H. et al., 1997. Miranda directs Prospero to a daughter cell during
559 Drosophila asymmetric divisions. *Nature Cell Biology*, 390(6660), pp.625–629.

560 Ito, K., Urban, J. & Technau, G.M., 1995. Distribution, classification, and development
561 ofDrosophila glial cells in the late embryonic and early larval ventral nerve cord. *Roux's*
562 *archives of developmental biology*, 204(5), pp.284–307.

563 Jordan, P. & Karess, R., 1997. Myosin light chain-activating phosphorylation sites are required
564 for oogenesis in Drosophila. *Journal of Cell Biology*, 139(7), pp.1805–1819.

565 Joy, T., Hirono, K. & Doe, C.Q., 2014. The RanGEF Bj1 promotes prospero nuclear export and
566 neuroblast self-renewal. *Developmental neurobiology*, pp.n/a–n/a.

567 Knoblich, J.A., 2008. Mechanisms of asymmetric stem cell division. *Cell*, 132(4), pp.583–597.

568 Kocsis, E. et al., 1991. Image averaging of flexible fibrous macromolecules: the clathrin
569 triskelion has an elastic proximal segment. *Journal of structural biology*, 107(1), pp.6–14.

570 Lai, S.-L. & Doe, C.Q., 2014. Transient nuclear Prospero induces neural progenitor
571 quiescence. *eLife*, 3.

572 Lee, C.-Y. et al., 2006. Brat is a Miranda cargo protein that promotes neuronal differentiation

and inhibits neuroblast self-renewal. *Developmental Cell*, 10(4), pp.441–449.

Lee, T. & Luo, L., 1999. Mosaic analysis with a repressible cell marker for studies of gene function in neuronal morphogenesis. *Neuron*, 22(3), pp.451–461.

Lu, B. et al., 1998. Partner of Numb colocalizes with Numb during mitosis and directs Numb asymmetric localization in Drosophila neural and muscle progenitors. *Cell*, 95(2), pp.225–235.

Marthiens, V. & ffrench-Constant, C., 2009. Adherens junction domains are split by asymmetric division of embryonic neural stem cells. *EMBO reports*, 10(5), pp.515–520.

Matsuzaki, F. et al., 1998. miranda localizes staufen and prospero asymmetrically in mitotic neuroblasts and epithelial cells in early Drosophila embryogenesis. *Development*, 125(20), pp.4089–4098.

Maurange, C., Cheng, L. & Gould, A.P., 2008. Temporal transcription factors and their targets schedule the end of neural proliferation in Drosophila. *Cell*, 133(5), pp.891–902.

Mollinari, C., Lange, B. & Gonzalez, C., 2002. Miranda, a protein involved in neuroblast asymmetric division, is associated with embryonic centrosomes of Drosophila melanogaster. *Biology of the cell / under the auspices of the European Cell Biology Organization*, 94(1), pp.1–13.

Munro, E., Nance, J. & Priess, J.R., 2004. Cortical flows powered by asymmetrical contraction transport PAR proteins to establish and maintain anterior-posterior polarity in the early C. elegans embryo. *Developmental Cell*, 7(3), pp.413–424.

Pampalona, J. et al., 2015. Time-lapse recording of centrosomes and other organelles in Drosophila neuroblasts. *Methods in cell biology*, 129, pp.301–315.

Petritsch, C. et al., 2003. The Drosophila myosin VI Jaguar is required for basal protein targeting and correct spindle orientation in mitotic neuroblasts. *Developmental Cell*, 4(2), pp.273–281.

Petronczki, M. & Knoblich, J.A., 2001. DmPAR-6 directs epithelial polarity and asymmetric cell division of neuroblasts in Drosophila. *Nature Cell Biology*, 3(1), pp.43–49.

Prehoda, K.E., 2009. Polarization of Drosophila neuroblasts during asymmetric division. *Cold Spring Harbor perspectives in biology*, 1(2), pp.a001388–a001388.

Ramat, A., Hannaford, M. & Januschke, J., 2017. Maintenance of Miranda localization in Drosophila Neuroblasts involves interaction with the cognate mRNA. *Current Biology*, in press.

Rapsomaniki, M.A. et al., 2012. easyFRAP: an interactive, easy-to-use tool for qualitative and quantitative analysis of FRAP data. *Bioinformatics (Oxford, England)*, 28(13), pp.1800–1801.

Rolls, M.M. et al., 2003. Drosophila aPKC regulates cell polarity and cell proliferation in neuroblasts and epithelia. *Journal of Cell Biology*, 163(5), pp.1089–1098.

Saitoh, M. et al., 1987. Selective inhibition of catalytic activity of smooth muscle myosin light chain kinase. *The Journal of biological chemistry*, 262(16), pp.7796–7801.

Schindelin, J. et al., 2012. Fiji: an open-source platform for biological-image analysis. *Nature methods*, 9(7), pp.676–682.

614 Shen, C.P. et al., 1998. Miranda as a multidomain adapter linking apically localized
615 Inscuteable and basally localized Staufen and Prospero during asymmetric cell division in
616 Drosophila. *Genes & Development*, 12(12), pp.1837–1846.

617 Shen, C.P., Jan, L.Y. & Jan, Y.N., 1997. Miranda is required for the asymmetric localization of
618 Prospero during mitosis in Drosophila. *Cell*, 90(3), pp.449–458.

619 Smith, C.A. et al., 2007. aPKC-mediated phosphorylation regulates asymmetric membrane
620 localization of the cell fate determinant Numb. *The EMBO journal*, 26(2), pp.468–480.

621 Sousa-Nunes, R., Chia, W. & Somers, W.G., 2009. Protein phosphatase 4 mediates
622 localization of the Miranda complex during Drosophila neuroblast asymmetric divisions.
623 *Genes & Development*, 23(3), pp.359–372.

624 Spana, E.P. & Doe, C.Q., 1995. The prospero transcription factor is asymmetrically localized
625 to the cell cortex during neuroblast mitosis in Drosophila. *Development*, 121(10),
626 pp.3187–3195.

627 Ueda, K. et al., 2002. Rho-kinase contributes to diphosphorylation of myosin II regulatory
628 light chain in nonmuscle cells. *Oncogene*, 21(38), pp.5852–5860.

629 Uemura, T. et al., 1989. numb, a gene required in determination of cell fate during sensory
630 organ formation in Drosophila embryos. *Cell*, 58(2), pp.349–360.

631 Watanabe, T., Hosoya, H. & Yonemura, S., 2007. Regulation of myosin II dynamics by
632 phosphorylation and dephosphorylation of its light chain in epithelial cells. *Molecular*
633 *biology of the cell*, 18(2), pp.605–616.

634 Winter, C.G. et al., 2001. Drosophila Rho-associated kinase (Drok) links Frizzled-mediated
635 planar cell polarity signaling to the actin cytoskeleton. *Cell*, 105(1), pp.81–91.

636 Wirtz-Peitz, F., Nishimura, T. & Knoblich, J.A., 2008. Linking cell cycle to asymmetric division:
637 Aurora-A phosphorylates the Par complex to regulate Numb localization. *Cell*, 135(1),
638 pp.161–173.

639 Wodarz, A. et al., 1999. Bazooka provides an apical cue for Inscuteable localization in
640 Drosophila neuroblasts. *Nature Cell Biology*, 402(6761), pp.544–547.

641 Wodarz, A. et al., 2000. Drosophila atypical protein kinase C associates with Bazooka and
642 controls polarity of epithelia and neuroblasts. *Journal of Cell Biology*, 150(6), pp.1361–
643 1374.

644 Zhang, F. et al., 2016. Phosphotyrosyl phosphatase activator facilitates localization of Miranda
645 through dephosphorylation in dividing neuroblasts. *Development*, 143(1), pp.35–44.

646

647

648

649

650

651

652 **Figures and Figure legends**

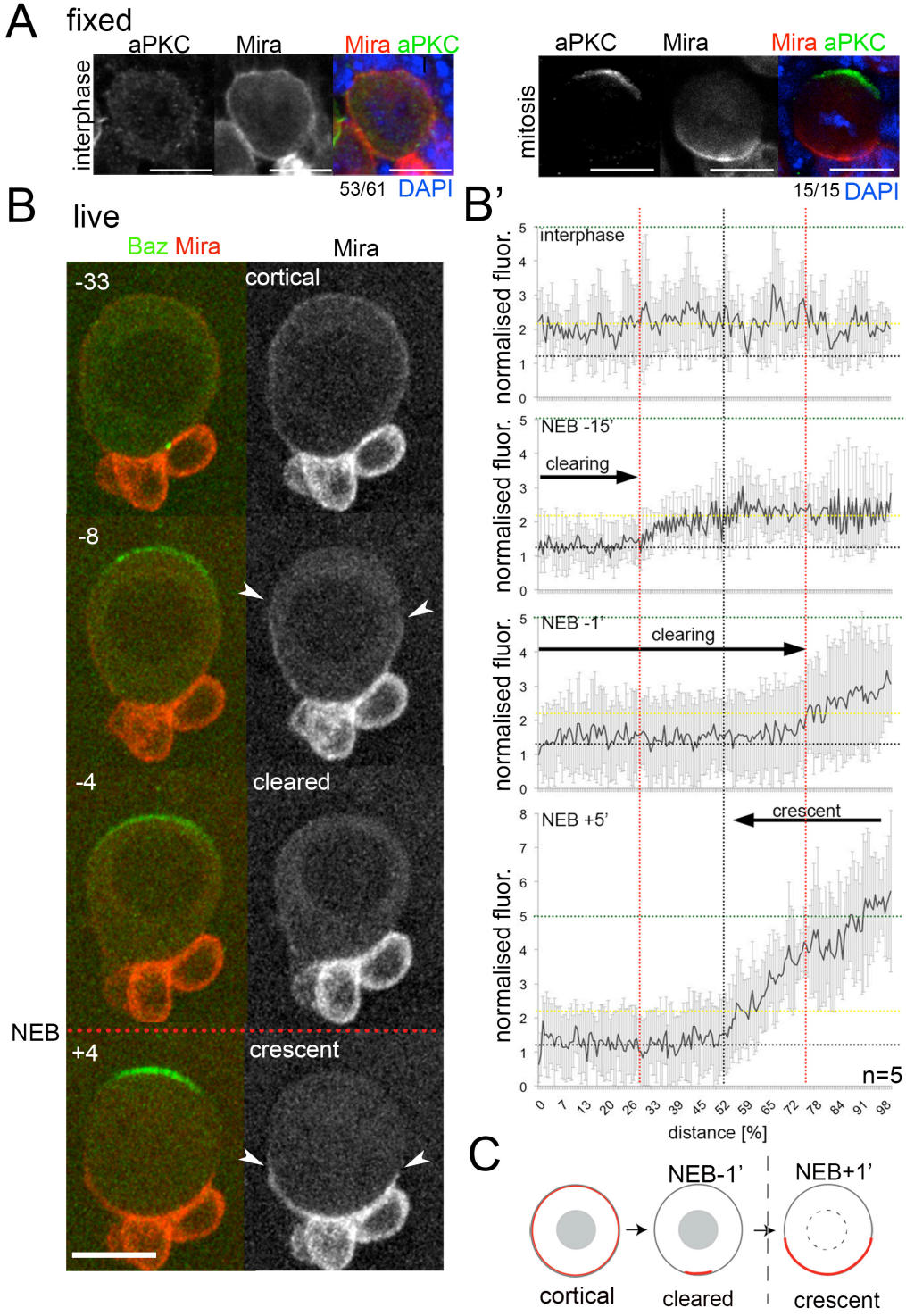

Figure 1

653

654 **Figure 1.** Miranda is cleared from the cortex before localizing in a basal
655 crescent in mitosis. (**A**) Larval brain NBs fixed and stained as labeled at the
656 indicated cell cycle stage. (**B**) Selected frames from **Movie S1**. NB in primary
657 cell culture expressing Baz::GFP (green) and Mira::mCherry (red) in the

transition from interphase to mitosis. Arrowheads point at Mira being cleared (-8) and at basal Mira crescent (+4). (**B'**) Quantification of cortical Mira::mCherry signal plotting the fluorescence intensities from the apical to the basal pole computationally straightening (Kocsis et al. 1991) the cortices of 5 NBs against the distance in %. Fluorescence was background subtracted and normalized to background subtracted cytoplasmic signal (1, dotted line). Cortical signal (yellow dotted line) and signal after NEB (green dotted line). Error bars, standard deviation. (**C**) Schematic of Mira localization. *BAC{mira::mcherry-MS2}* was the source of Mira::mCherry. Scale bar 10µm. Time stamp: minutes.

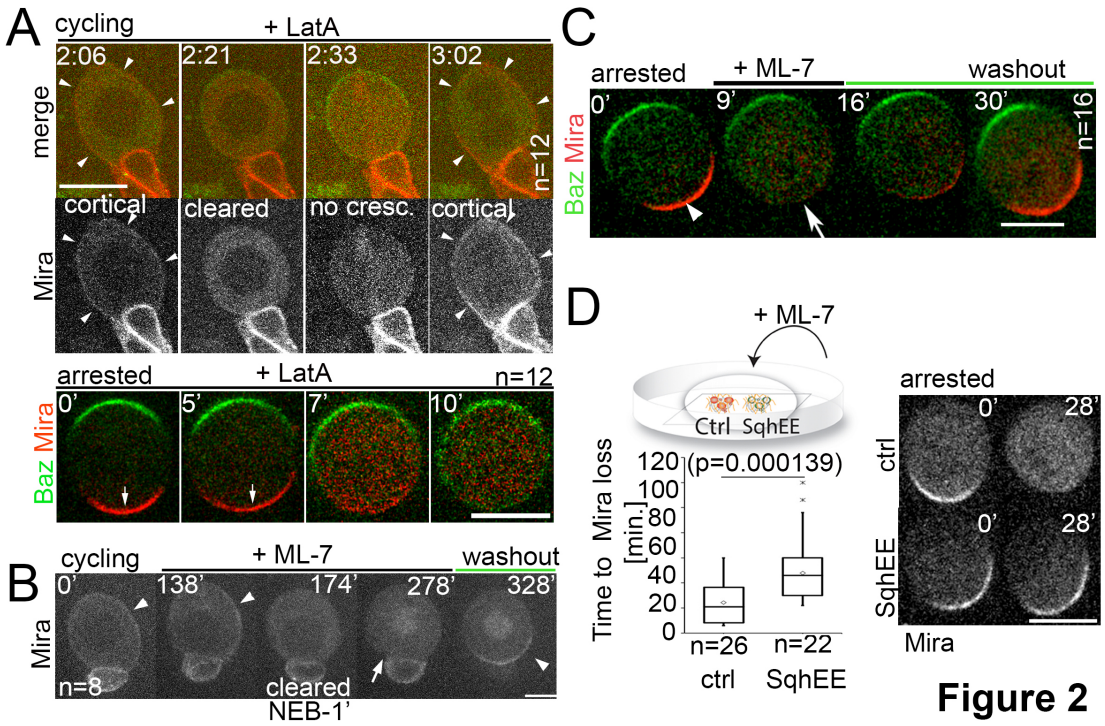

Figure 2

Figure 2. Differential response of Mira localization in interphase and mitosis to disruption of the actin cytoskeleton. (**A**) Stills from **Movie S3**. LatA was added to a cycling NB in primary cell culture expressing Baz::GFP (green) and Mira::mCherry (red). Arrowheads point at cortical Mira after culturing ~1h with LatA (2:06). At 1 min to NEB, Mira::mCherry is cleared from the cortex (2:21). Mira forms no crescent in the next mitosis (2:33), but after cytokinesis

fails (note bi-nucleated cell at 3:02), Mira is recruited to the cortex (arrowheads). Bottom panels: Colcemid arrested NBs expressing Baz::GFP and Mira::mCherry. 5µM LatA was added prior to imaging at 15sec. intervals. Mira crescents (arrows) are lost upon LatA treatment. (**B**) Cycling NB in primary cell culture expressing Mira::mCherry, that remains cortical upon ML-7 addition (15µM; interphase: 0' and 138', arrowheads), is cleared 1minute prior to NEB (174'), does not form a crescent after NEB (278', arrow), but accumulates on the spindle (seen in cross section). After ML-7 washout, a basal Mira::mCherry crescent recovers (arrowhead, 328'). (**C**) Related to **Movie S5.** Colcemid arrested NB in primary cell culture expressing Baz::GFP (green) and Mira::mCherry (red). After addition of 20µM ML-7 Mira (arrowhead, 0') becomes cytoplasmic (arrow, +9'), but upon ML-7 washout a Mira crescent recovers. (**D**) The effect of 20µM ML-7 can be quenched by overexpressing a phospho-mimetic form Sqh (Sqh^{EE}). Colcemid arrested NBs (ctrl: Mira::mCherry: SqhEE: Mira::mCherry co-expressing SqhEE by worniuGal4). Ctrl and SqhEE were co-cultured and ML-7 added (related to **Movie S6**). Quantification of the time required to cause Mira::mCherry to become cytoplasmic shown on the left. Two-tailed ttest for independent means revealed significance. *BAC{mira::mcherry-MS2}* was the source of Mira::mCherry. Scale bar: 10µm.

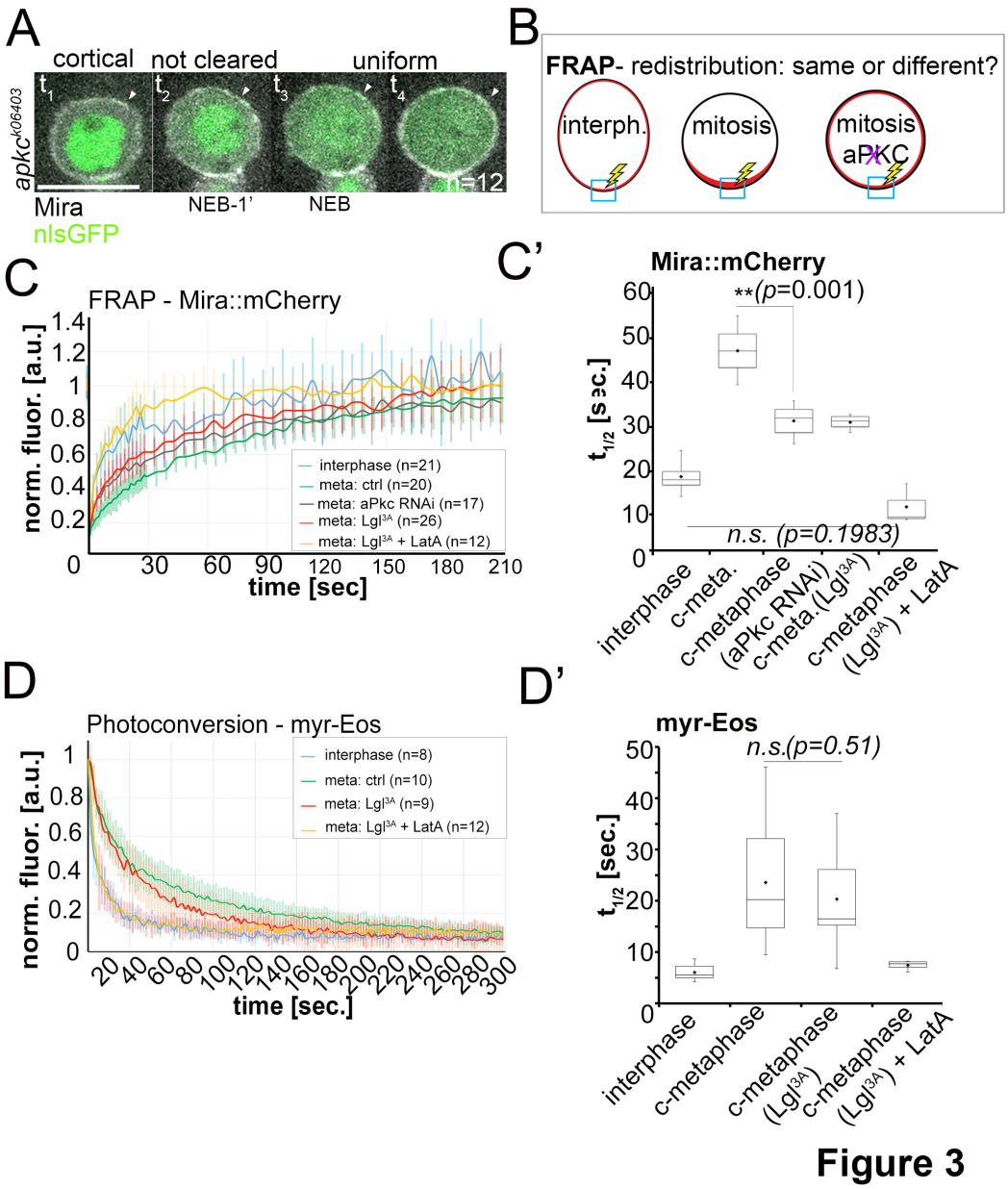

Figure 3

Figure 3. Lateral diffusion and cytoplasmic exchange of cortical Miranda are different in control and aPKC impaired mitotic NBs. (**A**) Stills from **Movie S7** of an *apkc*^{k06403} mutant NB (MARCM clone labeled with nlsGFP, green) expressing Mira::mCherry (grey). Mira is cortical in interphase, as the NB enters mitosis and after NEB (arrowheads, $t_1 - t_4$). (**B**) Conditions analyzed by FRAP. (**C**) Fluorescence redistribution curves of cortical Mira::mCherry at the indicated conditions. (**C'**) Estimates of $t_{1/2}$ [sec.] for cortical Mira::mCherry under the indicated conditions derived from curve fitting (Rapsomaniki et al.

711 2012). (**D**) Photo-conversion experiment monitoring loss of myr-EOS
712 converted signal over time. (**D'**) Estimates of $t_{1/2}$ [sec.] for cortical
713 Mira::mCherry under the indicated conditions from curve fitting.
714 Overexpression was driven by worniu-Gal4. p values: two-tailed ttest for
715 independent means. Scale bar: 10µm.
716

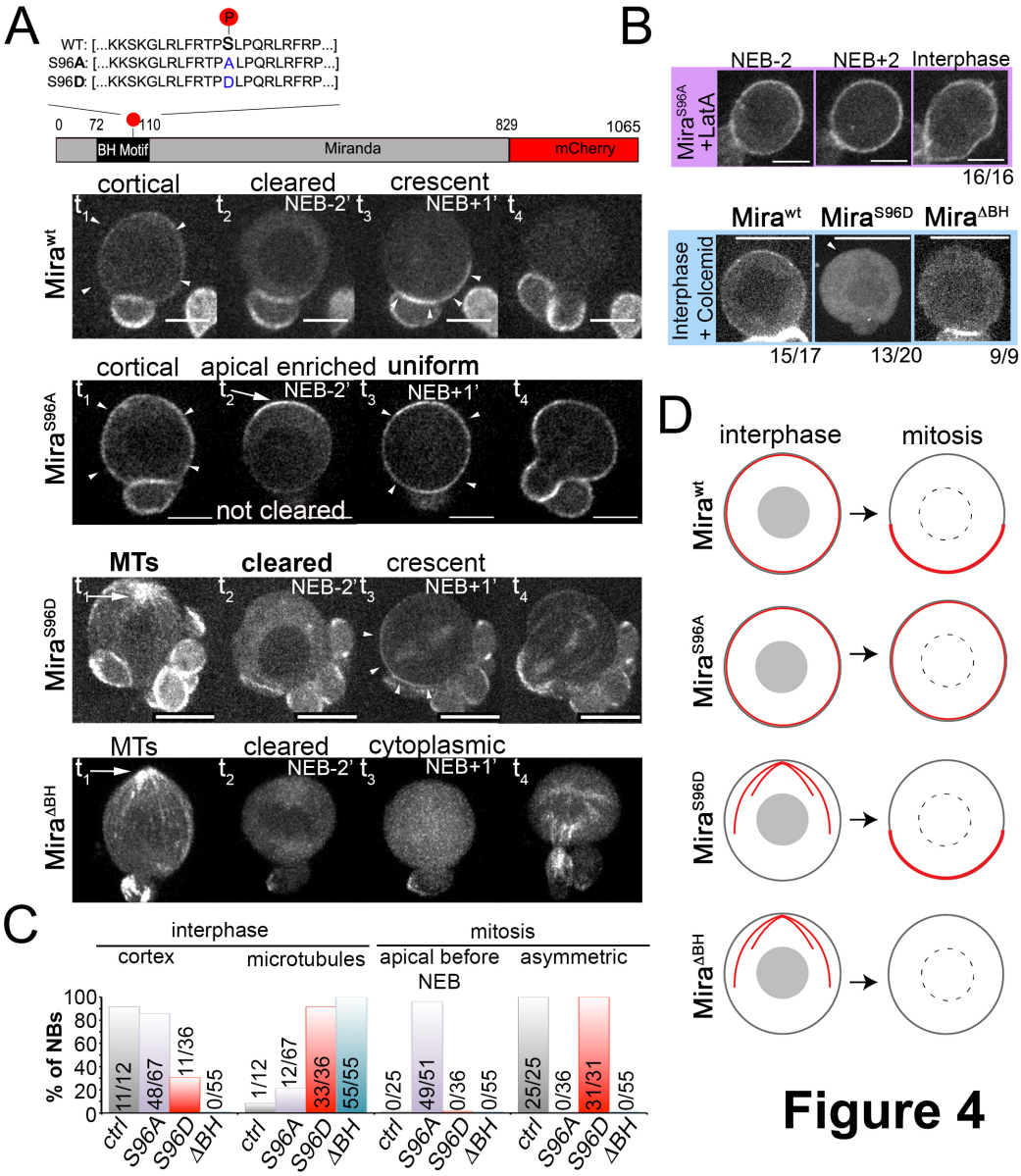

Figure 4

717

718 **Figure 4.** Miranda binds to the plasma membrane in interphase NBs via its
719 BH motif. (**A**) Schematic indicating the different Mira alleles used.
720 Mira::mCherry localizes cortically uniform in interphase (arrowheads t_1), is
721 cleared from the cortex shortly before NEB and forms a crescent (arrowheads
722 t_3) thereafter that is inherited by daughter cells (related to **Movie S8**). The

723 phosphomutant S96A is uniformly cortical in interphase, accumulates apically
724 shortly before NEB (arrow, t_2), is uniformly cortical after NEB (arrowheads t_3)
725 and in telophase (t_4, related to **Movie S9**). The phosphomimetic S96D
726 localizes to cortical microtubules in interphase (arrow t_1), is cleared from the
727 cortex before NEB and asymmetric after NEB (arrowheads t_3) and segregates
728 to daughter cells (related to **Movie S10**). Deletion of the BH motif leads to
729 cortical microtubule localization in interphase (arrow t_1), cytoplasmic
730 localization before and after NEB and reappearance on microtubules around
731 cytokinesis (related to **Movie S11**). (**B**) Neuroblasts expressing the indicated
732 Mira alleles were treated with 1µM LatA or 50µM colcemid for 60min. Cortical
733 localization of S96A is insensitive to LatA treatment. Below: While the Control
734 remains cortical, S96D and ΔBH become cytoplasmic upon colcemid
735 treatment. (**C**) Frequency of indicated localization of the different Mira
736 mutants. (**D**) Schematic of the localization of the different Mira alleles. Scale
737 bar: 10µm.
738

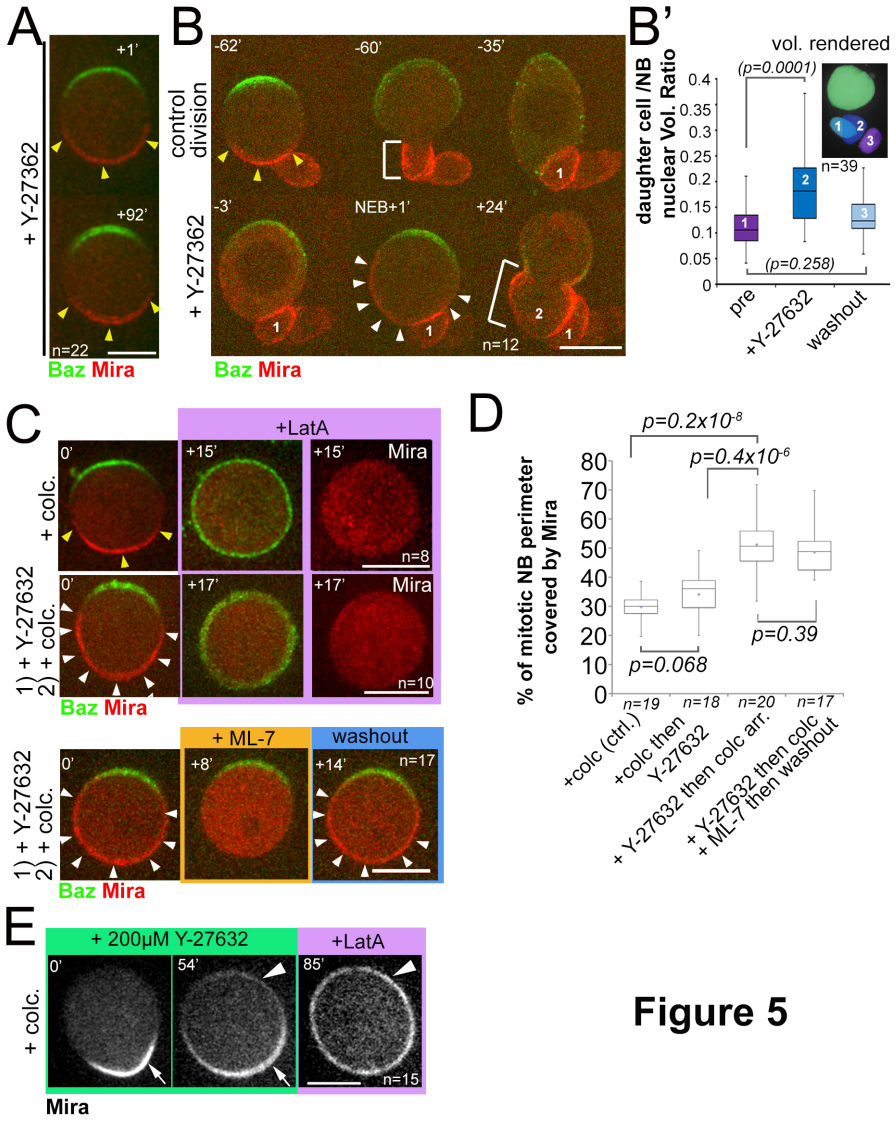

Figure 5

Figure 5. Mira crescent size is affected by a Y-27632-sensitive mechanism that operates before NEB. (**A**) Culturing colcemid arrested NBs in 50µM Y-27632 did not alter Mira crescent size (yellow arrowheads). (**B**) NBs polarizing in the presence of 25µM Y-27632 show enlarged Mira crescents. Control division (-62' to -35') with normally sized Mira crescent and daughter cell size (-60'; yellow arrowheads, bracket, respectively). Dividing in the presence of Y-27632 (-3, NEB+1) leads to an enlarged Mira crescent (NEB+1, white arrowheads) and enlarged daughter cell size (+24', brackets, 2). (**B'**) Plot of the ratio of daughter cell to NB nuclei as a measure for the effect of Y-27632 on daughter cell size. NBs expressing NLSGFP were imaged by DIC to follow daughter cell birth order during three consecutive divisions [1) pre-treatment; 2) div. in the presence of 25µM Y-27632; 3) div. after drug washout]. Then a

752 high-resolution z-stack of nlsGFP was recorded, and the nuclear volumes
753 rendered and calculated using IMARIS to plot their ratio. *p* values: Dunn's
754 test. (**C**) NBs were allowed to polarize in the absence (*upper row*) or presence
755 of 25µM Y-27632 (middle and lower row) followed by colcemid arrest. *upper*
756 *row*: Control NB with normal Mira crescent (yellow arrowheads) was
757 depolarized by 1µM LatA. Mira was displaced into the cytoplasm. *middle row*:
758 adding 1µM LatA leads to displacement of the enlarged Mira crescent (yellow
759 arrowheads) in the cytoplasm. *Lower row:* adding 20µM ML-7 drives Mira into
760 the cytoplasm (+8'). Upon ML-7 washout, Mira recovered to an enlarged
761 crescent (+14', white arrowheads). (**D**) Quantification of Mira crescent size in
762 the aforementioned experiments (unpaired ttest). (**E**) Colcemid arrested NBs
763 were treated with 200µM Y-276322. Mira remains asymmetric even after
764 56min in the drug. LatA addition (5µM) abolishes that asymmetric bias and
765 Mira is uniformly distributed on the membrane. *Time* stamp: min. Labels as
766 indicated. *BAC{mira::mcherry-MS2}* was the source of Mira::mCherry. Scale
767 bar: 10µm.
768
769
770
771
772
773
774
775
776
777
778
779
780
781
782
783

Figure supplements

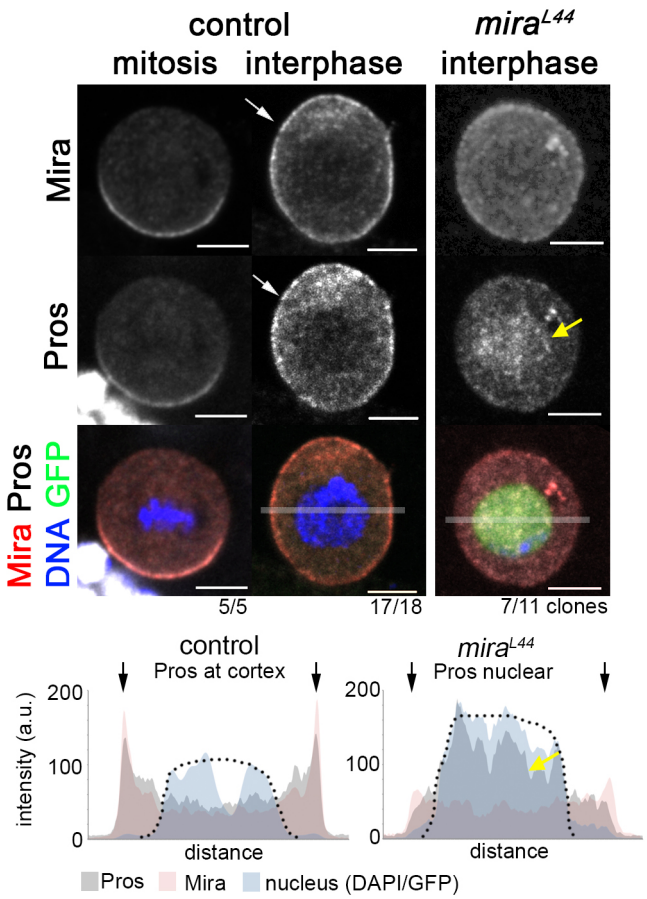

Figure 1 supplement 1

Figure 1 supplement 1. Uniform cortical Prospero depends on Miranda in interphase larval NBs. In w^{1118} brains, Mira and Pros form basal crescents in mitosis and both are cortical in interphase (arrow). In an interphase *mira*^{L44} NB (MARCM clone, GFP^{+}) cortical Mira and Pros are strongly reduced and Pros accumulates in the nucleus (yellow arrow). Transparent bars in merge interphase (control) and *mira*^{L44} indicate area used for plot profiles shown below. Pros and Mira are at the cortex (arrows) in the control and Pros is enriched in the nucleus in the mutant (yellow arrow). Arrows: outline of cell. Dotted line: nucleus (based on DAPI, control and GFP (MARCM clone). Scale bar: 10µm.

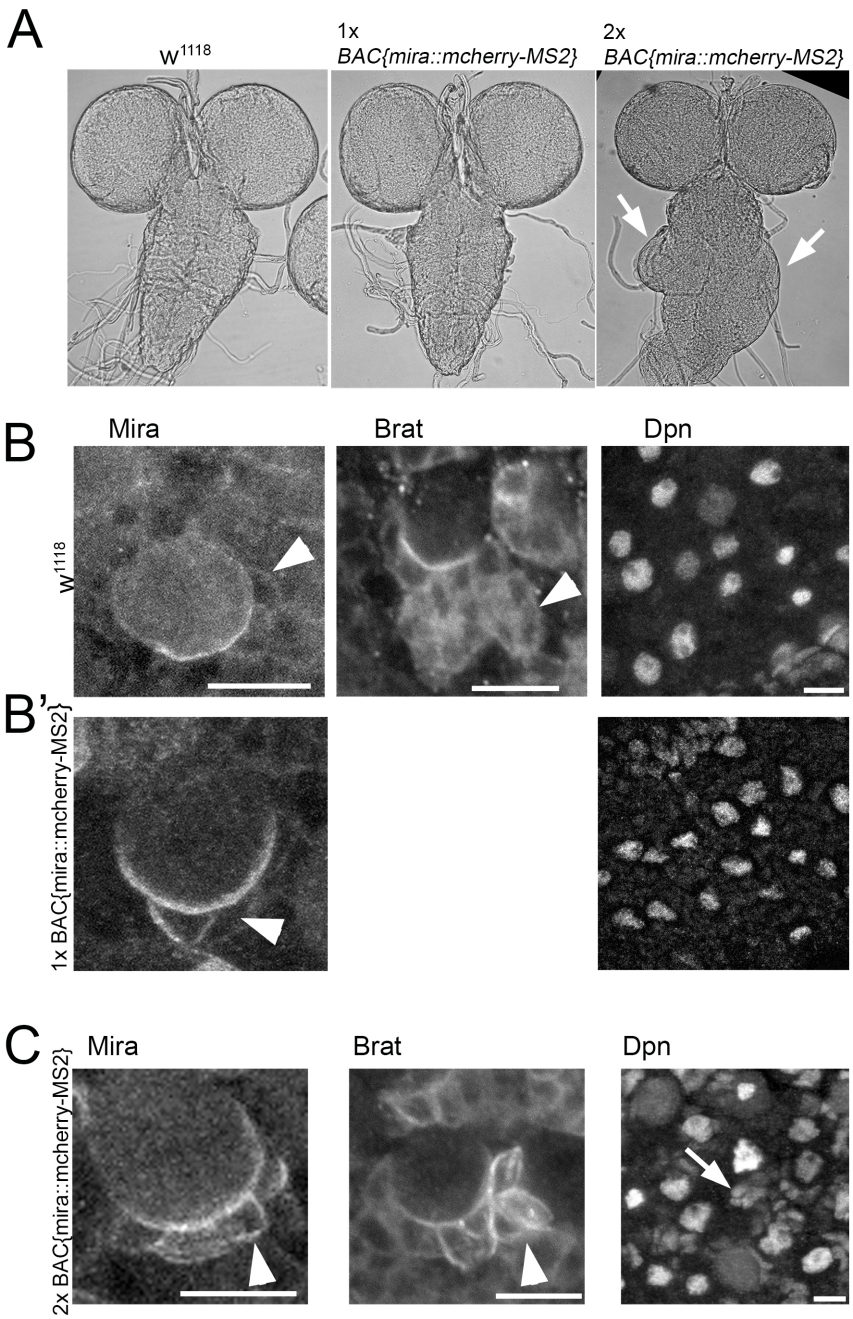

Figure 1 supplement 2

Figure 1 supplement 2. *BAC{mira::mcherry-MS2}* rescues embryonic lethality of the loss of function allele mira^{L44} over the deficiency DF(3R)ora^{I9}. However, animals die during puparium formation, when *BAC{mira::mcherry-MS2}* is the only source of Mira. (**A**) Brightfield images of fixed whole mount brain preparations. *w^{1118}* (control, n=5) a *BAC{mira::mcherry-MS2}* brain over a wild type chromosome (1x *BAC{mira::mcherry-MS2}, n=12*) and a brain from *BAC{mira::mcherry-MS2}* Df(3R)ora^{I9} over a unrecombined *mira^{BACmCherry}* chromosome (2x *BAC{mira::mcherry-MS2}, n=12*). 2x

BAC{mira::mcherry-MS2} animals die as pharates. The ventral ganglion (VG) of these brains is frequently overgrown (arrows). Similar effects are seen with CrispR generated, homozygous *mira::mCherry::HA* larvae (not shown). (**B**) In fixed w^{1118} brains Mira as well as its cargo Brat are diffuse in the cytoplasm of NB daughter cells and Deadpan (Dpn) staining is restricted to NB nuclei. (**B'**) *BAC{mira::mcherry-MS2}*brains are not overgrown, Mira is sometimes more stable at the cortex in a daughter cell (arrowhead), but Dpn is normal. (**C**) In 2x *BAC{mira::mcherry-MS2}* animals, Mira is strongly cortical in several NB daughter cells and so is Brat (arrowheads). Dpn is no longer restricted to NB nuclei but frequently found in clusters of smaller nuclei close to NBs suggesting that Mira is stabilized at the cortex and fails to release its cargo, inducing fate changes. mCherry is fused to the C-terminus of Mira which was shown to be required for cargo release (Fuerstenberg et al. 1998; Matsuzaki et al. 1998). Scale bars: 10µm.

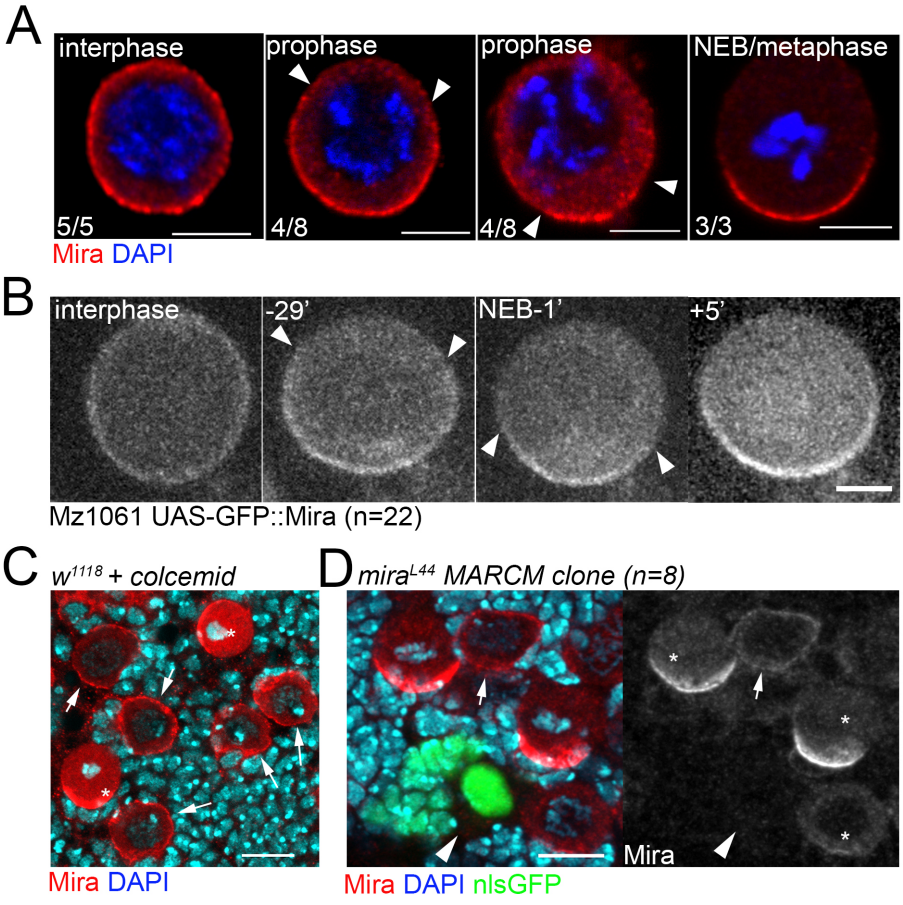

Figure 1 supplement 3

825 **Figure 1 supplement 3**. Cortical Mira can be detected by antibody staining,
826 in UAS-GFP-Mira overexpressing NBs and upon colcemid treatment, but not in
827 interphase mira^{L44} loss of function clones. (**A**) Antibody staining against Mira
828 performed on different fixed isolated NBs in primary cell culture. In this assay
829 Mira (red) is cortical in an interphase NB (judged by DAPI, blue). In prophase
830 NBs, differently sized Mira "crescents" can be detected the ends of which are
831 labeled by arrowheads. In a metaphase NBs Mira forms a crescent that
832 appears larger than some of those seen in prophase NBs. (**B**) A living NB in
833 primary cell culture expressing Mira::GFP driven by Mz1061. GFP signal is at
834 the cortex in interphase, 29 min prior to NEB, GFP signal becomes cleared
835 apically (arrowheads) until most of the cortex is cleared 1min prior to NEB. 5
836 min after NEB a robust, larger crescent has formed. (**C**) Control brain treated
837 with 50µM colcemid for 30min and stained for Mira. Over condensed
838 chromatin in mitotic NBs demonstrates the effect of colcemid yet in all
839 interphase NBs Mira remains at the cortex. (**D**) Fixed brain containing an
840 interphase NB MARCM *mira*^{L44} clone surrounded by control NBs. In the clone
841 cortical Mira signal is gone (arrowhead) while present in a control interphase
842 NB (arrow). Asterisks: mitotic NBs. Scale bar 10µm.
843
844

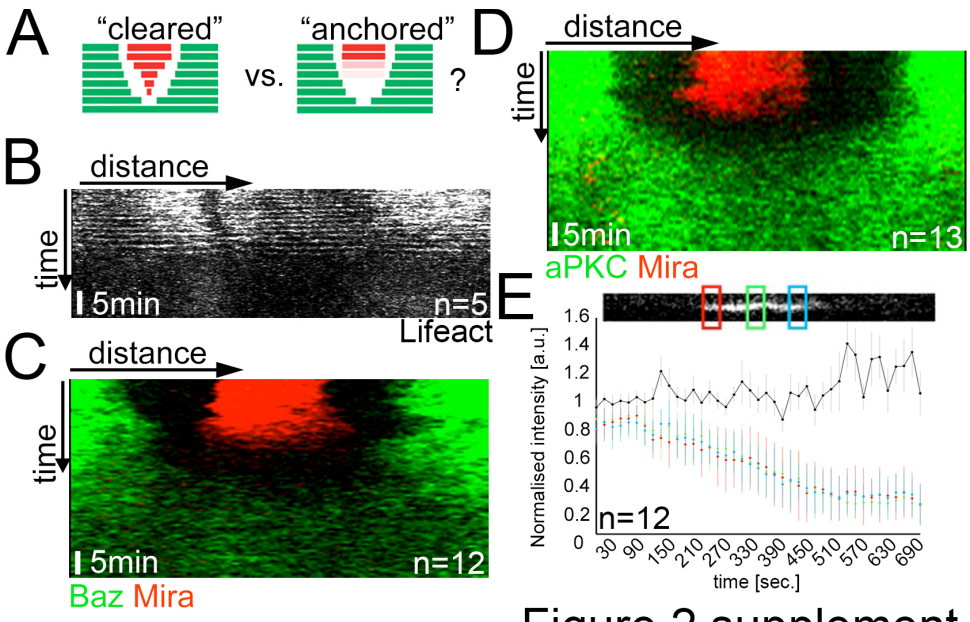

Figure 2 supplement

845

Figure 2 supplement. Mira falls homogenously off the cortex upon LatA treatment, which is not driven by aPKC cortical displacement. (**A**) Schematic depicting the expected kymograph profile for *clearing* versus *anchoring*. (**B-D**) Kymographs of colcemid arrested NBs expressing Lifeact-Ruby, Baz::GFP and Mira::mCherry or aPKC::GFP and Mira::mCherry (related to **Movie S4**) upon the addition of 5µM LatA. The equatorial perimeter of the NB was straightened out for each time point. Time scale bar: 5min. (**E**) Plot of Mira decline upon LatA treatment of a colcemid arrested NB using 3 ROIs (positions as indicated). Black line shows ratio ROI3/ROI2 over time, which remains constant. Error bars: standard deviation. *BAC{mira::mcherry-MS2}* was the source of Mira::mCherry. Scale bar: 10µm.

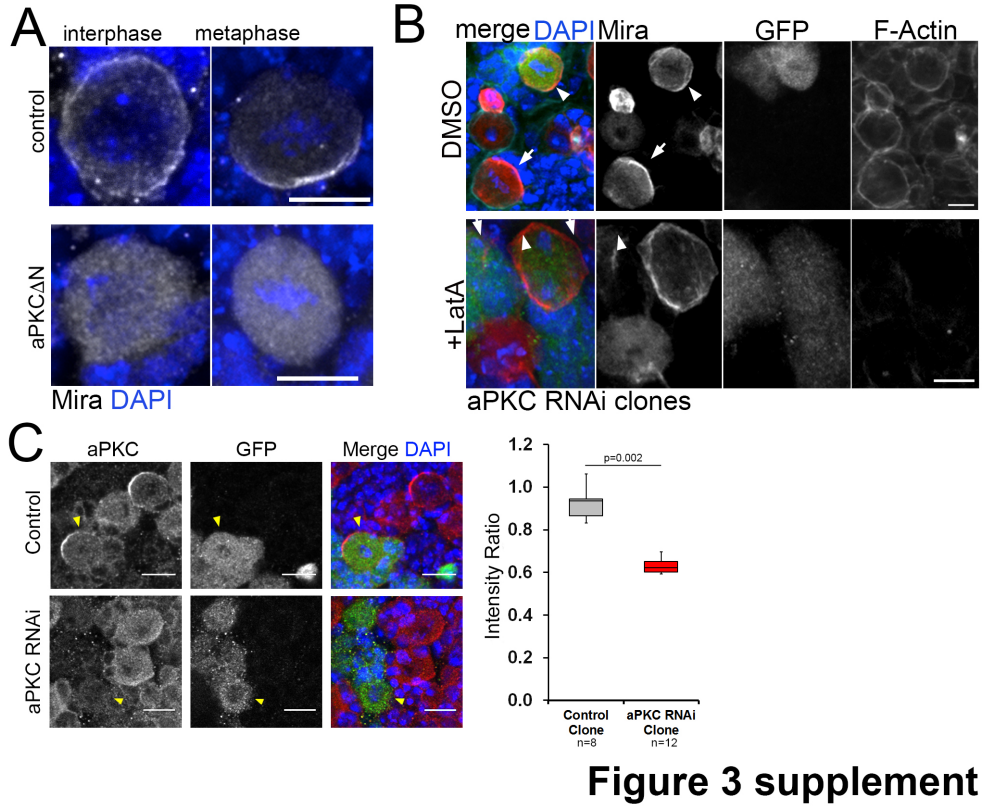

Figure 3 supplement

Figure 3 supplement. Effects of aPKC manipulation on Mira localization under different conditions. (**A**) Mira antibody staining on whole mount brains in a control NBs and in a NBs that expresses aPKC$^{\Delta N}$ by worniuGal4. Control:

865 Mira is cortical in interphase (91% cortex, 9% cytopl., n=53), forms a
866 crescent in metaphase (93% crescent, 7% cytopl., n=15). aPKC$^{\Delta N}$: Mira is
867 cytoplasmic in interphase (85% cytoplasm, 15% cortex, n=40) and
868 metaphase (89% cytopl., 11% crescent, n=15). (**B**) aPKC RNAi expressing
869 flip out clones (GFP positive, arrowheads) and GFP negative control NBs
870 (arrows) treated with DMSO or 5µM LatA and stained with an antibody
871 against Mira and with Phalloidin to label F-Actin. In GFP negative mitotic
872 control NBs, Mira is in a crescent (DMSO) or cytoplasmic (LatA). Mira is
873 cortical in DMSO as well as LatA treated mitotic aPKC RNAi NBs (100%, n=5,
874 arrowheads). (**C**) aPKC is efficiently knocked down by RNAi in flip out clones.
875 aPKC RNAi NBs have significantly less aPKC. Scale bar: 10µm.
876

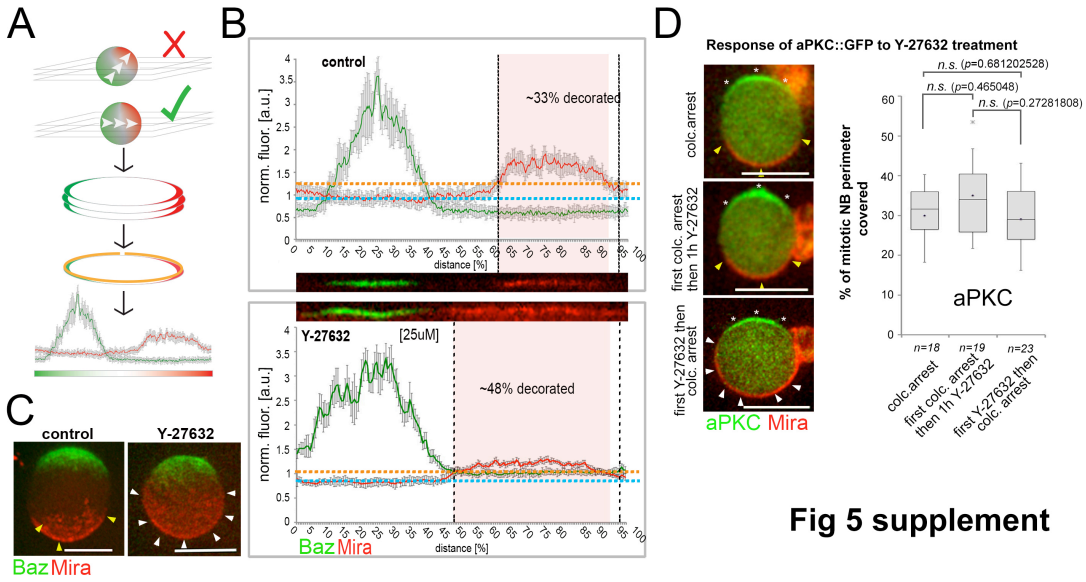

Fig 5 supplement

877
878

879 **Figure 5 supplement.** Standard used to quantify Mira crescent size. (**A**)
880 Schematic of workflow. NBs that have a polarity axis parallel to the imaging
881 plane are selected. 3-5 optical planes are collected covering 2-3µm of the
882 equator of the NB. (**B**) Fluorescence is normalized against the cytoplasmic
883 background and straightened line plots are derived from each section. The
884 average background and the average standard deviation is determined.
885 Signal: > avg. background plus two times the average standard deviation. (**C**)
886 3D projections of z-sections covering the entire NBs, ctrl vs. a NB that
887 polarized in the presence of 25µM Y-27632. (**D**) Quantification of aPKC::GFP

888 crescent size under the indicated conditions (unpaired ttest). Asterisks: aPKC;
889 yellow arrowheads: normal sized crescents; white arrowheads: enlarged Mira
890 crescents. *BAC{mira::mcherry-MS2}* was the source of Mira::mCherry. Scale
891 bar: 15µm.
892
893 **Movie captions**
894 **Movie S1**
895 Interphase cortical Miranda is removed at the onset of mitosis. Spinning disc
896 confocal image of a neuroblast expressing Baz::GFP (red) and Mira::mCherry
897 (green). For this and all subsequent videos maximum projection after a 3D
898 Gaussian blur (FIJI, radius 8/.8/1) of 7 consecutive equatorial planes taken at
899 0.4µm spacing is shown. Z-stacks taken every minute. Time stamp: hh:mm.
900
901 **Movie S2**
902 Interphase cortical Miranda is removed at the onset of mitosis. Spinning disc
903 confocal image of a neuroblast expressing aPKC::GFP (green) and
904 Mira::mCherry (red). Z-stacks taken every minute. Time stamp: hh:mm.
905
906 **Movie S3**
907 Interphase cortical Miranda is actin independent. Spinning disc confocal
908 image of a neuroblast expressing Baz::GFP (red) and Mira::mCherry (green)
909 showing a control division before 1µM LatA was added. Z-stacks taken ~every
910 minute. Z-stacks taken every minute. Time stamp: hh:mm.
911
912 **Movie S4**
913 Colcemid arrested NBs expressing aPKC::GFP and Mira::mCherry that were
914 treated with 5µM LatA at the beginning of the recording at 16sec intervals.
915 The cortex was straightened out and split at the apical pole such that
916 aPKC::GFP appears right and left and Mira in the centre. Fluorescence profiles
917 shown below. Note that Mira falls off homogenously from the cortex and
918 becomes cytoplasmic at 5:36 (red arrowhead), while the detectable borders
919 of cortical aPKC (green arrowheads) have not yet changed. Only from 7:12

onward aPKC rise above cytoplasmic levels where Mira was localized. Time stamp: mm:ss.

Movie S5

Myosin inhibition reversibly affects basal Mira anchoring in a polarized neuroblast. A colcemid arrested NB expressing Baz::GFP (green) and Mira::mCherry (red) in primary cell culture was treated with 20µM ML-7 which as washout when indicated. Left panel Baz::GFP, middle panel Mira::mCherry, right panel merge. Z-stacks taken every minute. Time stamp: mm:ss.

Movie S6

The effect of ML-7 on cortical Mira localization in mitosis can be delayed by overexpressing Sqh^{EE}. Mira::mCherry NBs (ctrl) and Mira::mCherry NBs co-expressing Sqh^{EE} (rescue) were co cultured in neighboring clots in the same dish and the effect of ML-7 on cortical Mira recorded. Z-stacks taken every two minutes. Time stamp: hh:mm.

Movie S7

Miranda remains at the cortex throughout the cell cycle in *apkc*^{k04603} mutant NBs. Spinning disc confocal image of an $apkc^{k04603}$ mutant NB, labeled with nlsGFP (green) expressing Mira::mCherry (white). Z-stacks taken every minute. Time stamp: hh:mm.

Movie S8

Control $mira^{mCherry}$ allele generated by CrispR/Cas9. Mira localizes to the interphase cortex, from where it is cleared before NEB. Then Mira re-localizes to a larger crescent. Therefore this allele and Mira::mCherry (BAC rescue) are undistinguishable in terms of Mira dynamics. This control further shows that the MS2 binding site in the BAC rescue construct does not interfere with Mira cortical dynamics. Time stamp: hh:mm.

Movie S9

Phosphomutant S96A allele of Mira tagged with mCherry at the C-terminus. Mira localizes uniformly to the interphase cortex. Shortly before NEB, S96A is apically enriched, before being uniformly cortical after NEB and during division. Time stamp: hh:mm.

Movie S10

Phosphomimetic S96D allele of Mira tagged with mCherry at the C-terminus. S96D localizes to microtubules in interphase, but is asymmetric in mitosis in mitosis. Note the signal resembling subcortical microtubules in interphase converging at the apical pole. After NEB a basal crescent is detectable. At 115:30 a z-stack spanning the entire NB was collected and the maximum projection is frozen. After this 50µM colcemid was added to reveal if Mira^{S96D}::mCherry binds to the cortex. Next frozen frame: similar stack after 30min in colc. Next frozen frame: 50 in colcemid – no cortical signal is detectable. Last frozen frame 65min in colcemid. Time stamp: mm:ss. Scale 15µm.

Movie S11

Mira requires its BH motif for interphase cortical localization (see main text) and basal localization in mitosis. The BH motif in Mira has been deleted by gene editing and this Mira mutant tagged with mCherry at the C-terminus (*mira*$^{\Delta BHmCherry}$). Mira$^{\Delta BH}$::mCherry when homozygous is found on the interphase microtubule network and in the cytoplasm during mitosis. Time stamp: hh:mm.

Movie S12

200µM Y-27632 induced uniform cortical Mira in mitosis localizes independently of an intact actin network. A Baz::GFP and Mira::mCherry expressing NBs was cultured in the presence of 200µM Y-27632, arrested with colcemid. 5µM LatA was added after the first frame of the movie. LatA

induces loss of Baz asymmetry, yet Mira remains cortical. Z-stacks shown. Z stacks taken every 2min. Time stamp: hh:mm.

Movie S13

Colcemid arrested NBs expressing Baz::GFP and Mira::mCherry, treated with 200µM Y-27632. Mira starts to become visible ~36min after Y-27632 addition in this example, but remaines asymmetrically distributed, until LatA is added. Z-stacks shown. Z stacks taken every 2min. Time stamp: mm:ss.

Competing interest declaration

The authors declare no competing financial interests.

Author contribution

M.H., A.R., N.L. and J.J. designed and carried out experiments and interpreted the data and M.H., N.L. and J.J. wrote the manuscript that was agreed upon by all authors.